Accepted Manuscript

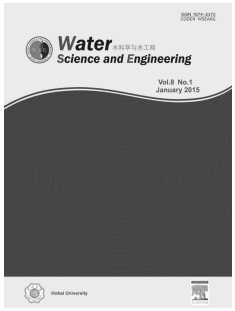

Free-surface long wave propagation over linear and parabolic transition shelves

Ikha Magdalena, Iryanto, Dominic E. Reeve

PII: S1674-2370(19)30001-8

DOI: https://doi.org/10.1016/j.wse.2019.01.001

Reference: WSE 161

To appear in: *Water Science and Engineering*

Received Date: 13 April 2018

Accepted Date: 19 September 2018

Please cite this article as: Magdalena, I., Iryanto, Reeve, D.E., Free-surface long wave propagation over linear and parabolic transition shelves, *Water Science and Engineering*, https://doi.org/10.1016/j.wse.2019.01.001.

Free-surface long wave propagation over linear and parabolic transition shelves

Ikha Magdalena [a], Iryanto [b], Dominic E. Reeve [c, *]

[a] *Faculty of Mathematics and Natural Sciences, Bandung Institute of Technology, Bandung 40132, Indonesia*
[b] *Informatics Department, Indramayu State Polytechnic, Indramayu 45252, Indonesia*
[c] *College of Engineering, Swansea University, Bay Campus, Swansea, SA2 8PP, UK*

Received 13 April 2018; accepted 19 September 2018
Available online xxx

Abstract

Long-period waves pose a threat to coastal communities as they propagate from deep ocean to shallow coastal waters. At the coastline, such waves have a greater height and longer period in comparison with local storm waves, and can cause severe inundation and damage. In this study, we considered linear long waves in a two-dimensional (vertical-horizontal) domain propagating towards a shoreline over a shallowing shelf. New solutions to the linear shallow water equations were found, through the separation of variables, for two forms of transition shelf morphology: deep water and shallow coastal water horizontal shelves connected by linear and parabolic transition, respectively. Expressions for the transmission and reflection coefficients are presented for each case. The analytical solutions were used to test the results from a novel computational scheme, which was then applied to extending the existing results relating to the reflected and transmitted components of an incident wave. The solutions and computational package provide new tools for coastal managers to formulate improved defence and risk-mitigation strategies.

Keywords: Shallow water equation; Long-period wave; Shoaling; Analytical solution; Numerical solution; Reflection coefficient; Transmission coefficient

1. Introduction

Deep water waves can undergo dramatic changes as they propagate towards a shoreline over an irregular seabed. The processes of refraction, shoaling, diffraction, and breaking can significantly alter wave heights and directions near the shore, and must be adequately accounted for in developing beach protection and flood defence. The wave period is also an important parameter in the design of coastal structures, particularly in relation to the process of shoaling. Long-period waves, such as tsunamis, storm surges, and swells, have greater wave lengths than local storm waves, and are therefore more susceptible to the effects of shoaling. Shoaling in particular can lead to reductions in wave length and speed, as well as amplification of wave height. As long waves propagate into the coastal zone over a shelving seabed, some of the wave energy will be reflected and some will be transmitted shoreward. The focus of this paper is on wave shoaling, as well as the transmission and reflection coefficients.

This topic has been the subject of extensive research through experiments, analytical methods, and numerical modeling. Approaches can be categorized broadly into the following three categories: two horizontal dimensions (2DH); vertical slices (2DV); and resolving the vertical and horizontal structures of the wave field (3D). Early analytical treatments, such as those of Carrier (1966) and Synolakis (1987), were 2DV and focused on predicting the run-up level of long waves. These have been supplemented by other analytical solutions accounting for refraction and friction (Nielson 1983, 1984) and cnoidal wave theories such as those in Sadeghian and Peyman (2012). A wide range of 2DV computational models have been developed and are based predominantly on the Boussinesq equations, the shallow water equations, or Reynolds-averaged Navier-Stokes (RANS) formulations. RANS modeling is the most computationally expensive of these equations and for that reason is limited to describing waves in a small domain such as the surf zone (e.g., Lin and Liu, 1998). There are comparatively fewer computational requirements for solving the Boussinesq equations. As a consequence, various forms of Boussinesq equations have been developed for both 2DV and 2DH applications. Early attempts were able to capture some nonlinear effects but encountered difficulties with accurate representation of linear dispersion properties at all water depths (e.g., Nwogu, 1993). More recent developments have allowed this deficiency to be addressed, at the cost of additional complexity (e.g., Madsen et al., 2002).

This work was supported by a Researcher Links Grant from the British Council, the Royal Academy of Engineering (Grant No. IAAP1/100086), and the EFRaCC Project funded through the British Council's Global Innovation Initiative Program.

* Corresponding author.
E-mail address: d.e.reeve@swansea.ac.uk (Dominic E. Reeve)

Early 2DH wave models were based on a form of the elliptic mild slope equation proposed by Berkhoff (1972), which account for refraction and diffraction and provide the variation of wave amplitude over a 2DH spatial domain. A more general time-dependent form was subsequently proposed by Smith and Sprinks (1975). The computational challenges of solving an elliptical wave equation led to the development of various parabolic approximations, such as those in Radder (1979), Kirby (1986), Ebersole (1985), and Panchang et al. (1988), as well as methods for solving the transient problem via a hyperbolic formulation (Copeland, 1985). An efficient means of solving the elliptic mild slope equation was proposed by Li and Anastasiou (1992), and extended by Li et al. (1993) to treat irregular wave propagation. Further developments of this theme have seen the inclusion of nonlinear effects by Beji and Nadoaka (1997); description of the wave field through an angular spectrum by Dalrymple et al. (1989), Suh et al. (1990), and Reeve (1992); and alternative derivations by Kim et al. (2009).

Here, we considered long waves occurring on a shelving foreshore and used the shallow water equations (SWEs) in a 2DV domain. Bautista et al. (2011) derived an analytical solution for long wave propagation over a linear transition shelf using a singular perturbation analysis based on the Wentzel-Kramers-Brillouin (WKB) technique. In this study, we derived analytical solutions to the linear SWEs based on the variable separation method and also developed a staggered finite volume method for their numerical solution.

This paper is organized as follows: Section 2 contains a brief description of the SWEs for waves propagating over linear and parabolic transition topography, and analytical solutions for the wave reflection and transmission coefficients are derived using the variable separation method, leading to solutions in terms of Bessel functions and polynomials; a staggered finite volume method for solving the SWEs over arbitrary topography is presented in Section 3; and in Section 4, we describe the implementation of our scheme to simulate wave propagation over linear and parabolic transition shelves. Moreover, to validate the numerical model, the computational solutions are compared with the analytical solutions and other results from previous studies. The validated numerical model is then applied to a topographic transect of the coast of Aceh, Indonesia. Conclusions are presented in the final section.

2. Shallow water model

2.1. Background

In this study, we considered a layer of ideal fluid, bounded above by a free surface and below by an impermeable bottom topography $z=-h(x)$, where x, z, and t are independent variables denoting the horizontal direction, vertical direction, and time, respectively. The following shallow water model for long waves in a relatively shallow region was adopted, following Kowalik (1993):

$$\begin{cases} \eta_t + (hu)_x = 0 \\ u_t + g\eta_x = 0 \end{cases} \tag{1}$$

where u is the horizontal velocity, η is the free surface elevation measured from the still water level, g is the gravitational acceleration, and h is the water depth. Eq. (1) represents the conservation of mass and momentum balance. The physical domain considered is shown in Fig. 1.

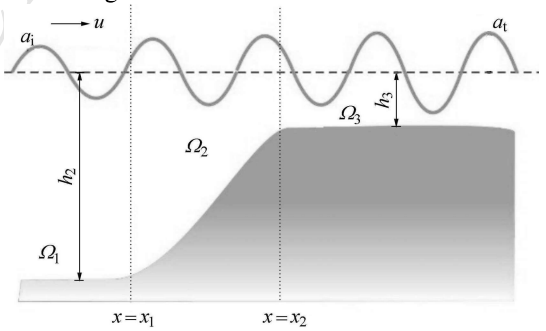

Fig. 1. Definition of model domain

The physical domain is divided into three different regions: Ω_1, Ω_2, and Ω_3, with prescribed depths defined by the following relationships:

(1) Linear transition shelf:

$$h(x)=\begin{cases} h_2 & x \le x_1 \\ h_2-\dfrac{h_2-h_3}{x_2-x_1}x & x_1 < x < x_2 \\ h_3 & x \ge x_2 \end{cases} \quad (2)$$

where x_1 and x_2 are the locations of the left and right borders of the second domain, respectively; and h_2 and h_3 are the depths in the first and third domains, respectively. For the linear transition shelf, we assumed that $x_1=0$ and $x_2=L$, where L is the horizontal extent of the sloping bottom.

(2) Parabolic transition shelf:

$$h(x)=\begin{cases} h_2 & x \le x_1 \\ ax^2 & x_1 < x < x_2 \\ h_3 & x \ge x_2 \end{cases} \quad (3)$$

where $h_2=ax_1^2$, $h_3=ax_2^2$, and a is an arbitrary parameter.

In the following two subsections, we derive the reflection and transmission coefficients of the free surface over the linear and parabolic transition shelves, respectively. When waves propagate over a shelf, they undergo a scattering process, with some of the wave energy being transmitted shoreward and some reflected back towards the deep sea. Analytical solutions of the SWEs can be derived based on multiple-scale asymptotic expansion (Mei et al., 2005; Noviantri and Pudjaprasetya, 2010) and the well-known WKB perturbation techniques (Bender and Orszag, 1978; Bautista et al., 2011). Here, solutions of the linear SWEs are derived using the variable separation method.

2.2. Reflected and transmitted waves for linear transition shelf

In domain Ω_1 the seabed is flat and the governing equations are as follows:

$$\begin{cases} \eta_t + h_2 u_x = 0 \\ u_t + g\eta_x = 0 \end{cases} \quad (4)$$

Using the variable separation method, the general solutions of $\eta(x,t)$ and $u(x,t)$ in domain Ω_1 are written for a monochromatic wave with unknown spatial dependence, $F(x)$ and $G(x)$, and arbitrary frequency ω:

$$\begin{cases} \eta(x,t)=F(x)\mathrm{e}^{-\mathrm{i}\omega t} \\ u(x,t)=G(x)\mathrm{e}^{-\mathrm{i}\omega t} \end{cases} \quad (5)$$

Substituting Eq. (5) into Eq. (4) yields the following:

$$\begin{cases} F_{xx}+\dfrac{\omega^2}{gh_2}F=0 \\ G(x)=\dfrac{g}{\mathrm{i}\omega}F_x \end{cases} \quad (6)$$

With the solution of $F(x)$, and by differentiating $F(x)$ with respect to x and substituting the result into Eq. (6), the solutions to Eq. (6) are obtained:

$$\begin{cases} F(x)=a_\mathrm{i}\,\mathrm{e}^{\mathrm{i}k_0x}+a_\mathrm{r}\,\mathrm{e}^{-\mathrm{i}k_0x} \\ G(x)=\dfrac{gk_0}{\omega}\left(a_\mathrm{i}\,\mathrm{e}^{\mathrm{i}k_0x}-a_\mathrm{r}\,\mathrm{e}^{-\mathrm{i}k_0x}\right) \end{cases} \quad (7)$$

where a_i is the amplitude of the incoming wave, and a_r is the amplitude of the reflected wave. The wave number, k_0, in domain Ω_1 obeys the following dispersion relation:

$$k_0^2=\frac{\omega^2}{gh_2} \quad (8)$$

Next, substituting Eq. (7) into Eq. (5) yields the following expressions for the free surface and velocity:

$$\begin{cases} \eta(x,t)=a_\mathrm{i}\,\mathrm{e}^{\mathrm{i}(k_0x-\omega t)}+a_\mathrm{r}\,\mathrm{e}^{-\mathrm{i}(k_0x+\omega t)} \\ u(x,t)=\sqrt{\dfrac{g}{h_2}}\left[a_\mathrm{i}\,\mathrm{e}^{\mathrm{i}(k_0x-\omega t)}-a_\mathrm{r}\,\mathrm{e}^{-\mathrm{i}(k_0x+\omega t)}\right] \end{cases} \quad (9)$$

In domain Ω_2 the governing equations for the linear transition region become

$$\begin{cases} \eta_t + \left[\left(h_2 - \dfrac{h_2 - h_3}{L}x\right)u\right]_x = 0 \\ u_t + g\eta_x = 0 \end{cases} \tag{10}$$

As in domain Ω_1, a general solution in the form given in Eq. (5) is sought. Substituting Eq. (5) into Eq. (10) yields

$$\begin{cases} \left(h_2 - \dfrac{h_2 - h_3}{L}x\right)F_{xx} - \dfrac{h_2 - h_3}{L}F_x + \dfrac{\omega^2}{g}F = 0 \\ G(x) = \dfrac{g}{\mathrm{i}\omega}F_x \end{cases} \tag{11}$$

Eq. (11) is the Bessel equation and its general solution can be written as $F(x) = C_1 J_0\left(2\sqrt{\omega^2 L\gamma}\right) + C_2 Y_0\left(2\sqrt{\omega^2 L\gamma}\right)$, with $\gamma = \sqrt{\dfrac{(L-x)h_2 + xh_3}{g(h_2 - h_3)}}$, where J_0 and Y_0 are the zero-order Bessel functions of the first and second kinds, respectively; and C_1 and C_2 are constants yet to be determined. Substituting $F(x)$ into Eq. (5) yields the solutions for the free surface and velocity in this region:

$$\begin{cases} \eta(x,t) = C_1 J_0\left(2\sqrt{\omega^2 L\gamma}\right)\mathrm{e}^{-\mathrm{i}\omega t} + C_2 Y_0\left(2\sqrt{\omega^2 L\gamma}\right)\mathrm{e}^{-\mathrm{i}\omega t} \\ u(x,t) = \dfrac{g}{\mathrm{i}\omega}\dfrac{\sqrt{\omega^2 L}}{\gamma g(h_2 - h_3)}\left[C_1 J_1\left(2\sqrt{\omega^2 L\gamma}\right)\mathrm{e}^{-\mathrm{i}\omega t} + C_2 Y_1\left(2\sqrt{\omega^2 L\gamma}\right)\mathrm{e}^{-\mathrm{i}\omega t}\right] \end{cases} \tag{12}$$

where J_1 and Y_1 are the first-order Bessel functions of the first and second kinds, respectively.

Considering an incoming wave from the deep-water area with depth h_2 propagating shoreward, the wave is partially reflected and partially transmitted while passing through the linear transition shelf. In the nearshore region Ω_3, where the water depth is shallow, there is only a transmitted wave (propagating to the right, as shown in Fig. 1), with an amplitude a_t, and the solution is given by

$$\begin{cases} \eta(x,t) = a_t\,\mathrm{e}^{\mathrm{i}[k_1(x-L)-\omega t]} \\ u(x,t) = \sqrt{\dfrac{g}{h_3}}a_t\,\mathrm{e}^{\mathrm{i}[k_1(x-L)-\omega t]} \end{cases} \tag{13}$$

where k_1 obeys the following dispersion relation:

$$k_1^2 = \frac{\omega^2}{gh_3} \tag{14}$$

In general, accounting for the transmitted and reflected parts of the incident wave train, the free surface $\eta(x,t)$ and horizontal velocity $u(x,t)$ throughout the domain can be formulated as follows:

$$\eta(x,t) = \begin{cases} a_i\,\mathrm{e}^{\mathrm{i}(k_0 x - \omega t)} + a_r\,\mathrm{e}^{-\mathrm{i}(k_0 x + \omega t)} & x \le 0 \\ C_1 J_0\left(2\sqrt{\omega^2 L\gamma}\right)\mathrm{e}^{-\mathrm{i}\omega t} + C_2 Y_0\left(2\sqrt{\omega^2 L\gamma}\right)\mathrm{e}^{-\mathrm{i}\omega t} & 0 < x < L \\ a_t\,\mathrm{e}^{\mathrm{i}[k_1(x-L)-\omega t]} & x \ge L \end{cases} \tag{15}$$

$$u(x,t) = \begin{cases} \sqrt{\dfrac{g}{h_2}}\left[a_i\,\mathrm{e}^{\mathrm{i}(k_0 x - \omega t)} - a_r\,\mathrm{e}^{-\mathrm{i}(k_0 x + \omega t)}\right] & x \le 0 \\ \dfrac{g}{\mathrm{i}\omega}\dfrac{\sqrt{\omega^2 L}}{\gamma g(h_2 - h_3)}\left[C_1 J_1\left(2\sqrt{\omega^2 L\gamma}\right)\mathrm{e}^{-\mathrm{i}\omega t} + C_2 Y_1\left(2\sqrt{\omega^2 L\gamma}\right)\mathrm{e}^{-\mathrm{i}\omega t}\right] & 0 < x < L \\ \sqrt{\dfrac{g}{h_3}}a_t\,\mathrm{e}^{\mathrm{i}[k_1(x-L)-\omega t]} & x \ge L \end{cases} \tag{16}$$

At the points $x = 0$ and $x = L$, where the three regions connect, matching conditions must be used to conserve the free surface and horizontal momentum across the whole domain. There are, therefore, four equations with four unknown variables in the matrix form, which may be written as $\boldsymbol{Ax} = \boldsymbol{b}$, where

$$\boldsymbol{A}=\begin{bmatrix} -1 & J_0\left(2\sqrt{\omega^2 L}\gamma_1\right) & Y_0\left(2\sqrt{\omega^2 L}\gamma_1\right) & 0 \\ 1 & \beta_1 J_1\left(2\sqrt{\omega^2 L}\gamma_1\right) & \beta_1 Y_1\left(2\sqrt{\omega^2 L}\gamma_1\right) & 0 \\ 0 & J_0\left(2\sqrt{\omega^2 L}\gamma_2\right) & Y_0\left(2\sqrt{\omega^2 L}\gamma_2\right) & -1 \\ 0 & \beta_2 J_1\left(2\sqrt{\omega^2 L}\gamma_2\right) & \beta_2 Y_1\left(2\sqrt{\omega^2 L}\gamma_2\right) & -1 \end{bmatrix}$$

$$\boldsymbol{x}=\begin{bmatrix} a_{\mathrm{r}} \\ C_1 \\ C_2 \\ a_{\mathrm{t}} \end{bmatrix} \qquad \boldsymbol{b}=\begin{bmatrix} a_{\mathrm{i}} \\ a_{\mathrm{i}} \\ 0 \\ 0 \end{bmatrix} \tag{17}$$

with

$$\beta_1=\sqrt{\frac{Lh_2}{g}}\frac{1}{\mathrm{i}\gamma_1(h_2-h_3)} \qquad \gamma_1=\gamma\big|_{x=0}$$

$$\beta_2=\sqrt{\frac{Lh_3}{g}}\frac{1}{\mathrm{i}\gamma_2(h_2-h_3)} \qquad \gamma_2=\gamma\big|_{x=L}$$

The solution of the equations above is $\boldsymbol{x}=\boldsymbol{A}^{-1}\boldsymbol{b}$. This leads to the wave reflection and transmission coefficients that are respectively defined as

$$C_{\mathrm{R}}=\frac{a_{\mathrm{r}}}{a_{\mathrm{i}}}=\frac{N_{21}M_1+N_{22}M_2}{N_{11}M_1+N_{12}M_2} \tag{18}$$

$$C_{\mathrm{T}}=\frac{a_{\mathrm{t}}}{a_{\mathrm{i}}}=\frac{2}{N_{11}M_1+N_{12}M_2} \tag{19}$$

where N_{11}, N_{12}, N_{21}, N_{22}, M_1, and M_2 are defined as follows:

$$N_{11}=J_0\left(2\sqrt{\omega^2 L}\gamma_1\right)+\beta_1 J_1\left(2\sqrt{\omega^2 L}\gamma_1\right)$$

$$N_{12}=Y_0\left(2\sqrt{\omega^2 L}\gamma_1\right)+\beta_1 Y_1\left(2\sqrt{\omega^2 L}\gamma_1\right)$$

$$N_{21}=J_0\left(2\sqrt{\omega^2 L}\gamma_1\right)-\beta_1 J_1\left(2\sqrt{\omega^2 L}\gamma_1\right)$$

$$N_{22}=Y_0\left(2\sqrt{\omega^2 L}\gamma_1\right)-\beta_1 Y_1\left(2\sqrt{\omega^2 L}\gamma_1\right)$$

$$M_1=\frac{Y_0\left(2\sqrt{\omega^2 L}\gamma_2\right)+\beta_2 Y_1\left(\sqrt{\omega^2 L}\gamma_2\right)}{\beta_2\left[J_0\left(2\sqrt{\omega^2 L}\gamma_2\right)Y_1\left(\sqrt{\omega^2 L}\gamma_2\right)+J_1\left(2\sqrt{\omega^2 L}\gamma_2\right)Y_0\left(\sqrt{\omega^2 L}\gamma_2\right)\right]}$$

$$M_2=\frac{J_0\left(2\sqrt{\omega^2 L}\gamma_2\right)+\beta_2 J_1\left(\sqrt{\omega^2 L}\gamma_2\right)}{\beta_2\left[J_1\left(2\sqrt{\omega^2 L}\gamma_2\right)Y_0\left(\sqrt{\omega^2 L}\gamma_2\right)+J_0\left(2\sqrt{\omega^2 L}\gamma_2\right)Y_1\left(\sqrt{\omega^2 L}\gamma_2\right)\right]}$$

Explicit expressions for the coefficients C_1 and C_2 are given in the matrix $\boldsymbol{x}$ in Eq. (17).

2.3. Reflected and transmitted waves for parabolic transition shelf

Approaches similar to those explained in Subsection 2.1 are used to find the wave reflection and transmission coefficients for a parabolic transition shelf. The free surface elevation and horizontal velocity in domains Ω_1 and Ω_3 are expressed as follows:

$$\eta(x,t)=\begin{cases} a_{\mathrm{i}}\,\mathrm{e}^{\mathrm{i}\left[k_0(x-x_1)-\omega t\right]}+a_{\mathrm{r}}\,\mathrm{e}^{-\mathrm{i}\left[k_0(x-x_1)+\omega t\right]} & x\le x_1 \\ a_{\mathrm{t}}\,\mathrm{e}^{\mathrm{i}\left[k_1(x-x_2)-\omega t\right]} & x\ge x_2 \end{cases} \tag{20}$$

$$u(x,t)=\begin{cases} \sqrt{\dfrac{g}{h_2}}\left(a_{\mathrm{i}}\,\mathrm{e}^{\mathrm{i}\left[k_0(x-x_1)-\omega t\right]}-a_{\mathrm{r}}\,\mathrm{e}^{-\mathrm{i}\left[k_0(x-x_1)+\omega t\right]}\right) & x\le x_1 \\ \sqrt{\dfrac{g}{h_3}}\,a_{\mathrm{t}}\,\mathrm{e}^{\mathrm{i}\left[k_1(x-x_2)-\omega t\right]} & x\ge x_2 \end{cases} \tag{21}$$

In domain Ω_2, the governing equations for the shelf with parabolic transition topography $h(x)=ax^2$ read as follows:

$$\begin{cases}\eta_t+\left(ax^2u\right)_x=0\\ u_t+g\eta_x=0\end{cases} \tag{22}$$

These equations may be solved within domain Ω_2 in exactly the same manner as before. Seeking solutions of $\eta(x,t)$ and $u(x,t)$ of the form given in Eq. (5) and substituting the results into Eq. (22) yield

$$\begin{cases}ax^2gF_{xx}+2agxF_x+\omega^2F=0\\ G(x)=\dfrac{g}{\mathrm{i}\omega}F_x\end{cases} \tag{23}$$

The solution of $F(x)$ in Eq. (23) is

$$F(x)=C_1x^{-\frac{1}{2}+\frac{b}{2}}+C_2x^{-\frac{1}{2}-\frac{b}{2}} \tag{24}$$

where $b=\sqrt{1-4\omega^2/(ga)}$, and the constant coefficients C_1 and C_2 remain to be determined. Substituting $F(x)$ into Eq. (23) yields

$$\begin{cases}\eta(x,t)=C_1x^{-\frac{1}{2}+\frac{b}{2}}\mathrm{e}^{-\mathrm{i}\omega t}+C_2x^{-\frac{1}{2}-\frac{b}{2}}\mathrm{e}^{-\mathrm{i}\omega t}\\ u(x,t)=\dfrac{g}{\mathrm{i}\omega}\left[\left(-\dfrac{1}{2}+\dfrac{b}{2}\right)C_1x^{-\frac{3}{2}+\frac{b}{2}}\mathrm{e}^{-\mathrm{i}\omega t}-\left(\dfrac{1}{2}+\dfrac{b}{2}\right)C_2x^{-\frac{3}{2}-\frac{b}{2}}\mathrm{e}^{-\mathrm{i}\omega t}\right]\end{cases} \tag{25}$$

The matching conditions are also used to conserve the free surface $\eta(x,t)$ and the horizontal momentum $h(x)u(x,t)$ along the discontinuity points, $x=x_1$ and $x=x_2$, which give us four equations with four unknown variables, a_r, a_t, C_1, and C_2. By determining a_r and a_t and the coefficients C_1 and C_2, we obtain the following reflection and transmission coefficients for wave propagation over a parabolic transition shelf:

$$C_\mathrm{R}=\frac{a_\mathrm{r}}{a_\mathrm{i}}=\frac{\mu^{\frac{b}{2}}-\left(\sqrt{b^2-1}-b\right)\mu^{-\frac{b}{2}}}{b\left[\left(\sqrt{b^2-1}\right)\mu^{\frac{b}{2}}+\left(-\sqrt{b^2-1}+b\right)\mu^{-\frac{b}{2}}\right]} \tag{26}$$

$$C_\mathrm{T}=\frac{a_\mathrm{t}}{a_\mathrm{i}}=\frac{2}{\left(\sqrt{b^2-1}+b\right)\mu^{-\frac{1}{2}+\frac{b}{2}}+\left(-\sqrt{b^2-1}+b\right)\mu^{-\frac{1}{2}-\frac{b}{2}}} \tag{27}$$

where $\mu=x_1/x_2$.

For the linear transition case, Fig. 2(a) and (b) show the variations of C_R with L and h_2/h_3, respectively, and Fig. 2(c) and (d) show the variations of C_T with L and h_2/h_3, respectively. C_R and C_T are virtually independent of L for the range 1 m < L < 10 m. C_R rises as h_2/h_3 increases to about 3.5, and then decreases slightly as h_2/h_3 increases further. In contrast, C_T rises monotonically with h_2/h_3.

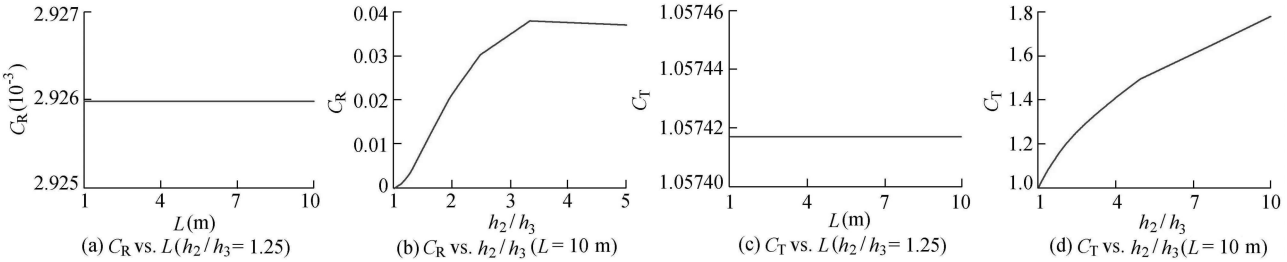

(a) C_R vs. $L(h_2/h_3=1.25)$ (b) C_R vs. h_2/h_3 ($L=10$ m) (c) C_T vs. $L(h_2/h_3=1.25)$ (d) C_T vs. h_2/h_3($L=10$ m)

Fig. 2. C_R and C_T as functions of h_2/h_3 and L, respectively, for linear transition shelf with $\omega=1.1922$ s^{-1}

Corresponding results for C_R and C_T, as functions of $\omega^2/(ga)$, for the parabolic transition case are shown in Fig. 3(a) and (b). The trend is that C_T increases with $\omega^2/(ga)$, μ, or h_2/h_3, meaning that more wave energy propagates towards the coast with the increases of $\omega^2/(ga)$, μ, and h_2/h_3. Fig. 4 shows that C_T, as a function of h_2/h_3, exhibits similar variations for both the parabolic and linear transition cases, which is also in close agreement with the analytical result of Kajiura (1961).

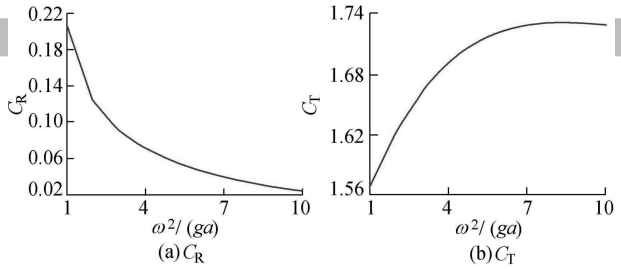

Fig. 3. C_R and C_T as functions of $\omega^2/(ga)$ for parabolic transition case when $\mu = 3.0$

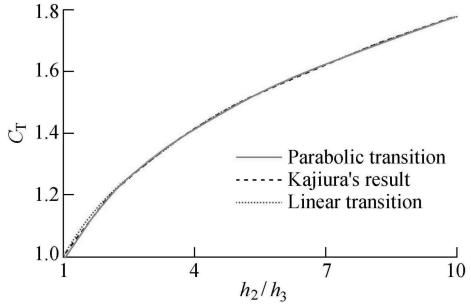

Fig. 4. C_T as function of h_2/h_3 for linear and parabolic transition cases, respectively, when $L = 10$ m and $\omega = 1.1922$ s^{-1}

3. Computational model

In this section, the numerical solution of Eq. (1), using a staggered conservative scheme, is presented. The scheme was described in detail in Pudjaprasetya and Magdalena (2014) and Magdalena et al. (2015). For the sake of concision, the scheme is described briefly here. We consider a computational domain Ω, consisting of a spatial domain $\Omega_L = [L_0, L_1]$ and a time domain $\Omega_T = [0, T]$. The spatial domain Ω_L is partitioned in a staggered way into several cells with a spatial step Δx. The time domain Ω_T is discretized into finite time steps with a constant interval Δt. Momentum and mass conservation equations (Eq. (1)) are discretized with cells centred at x_i and $x_{i+1/2}$, respectively. Furthermore, the water surface, η, and velocity, u, are defined at full- and half-grid points, respectively, as given in Fig. 5.

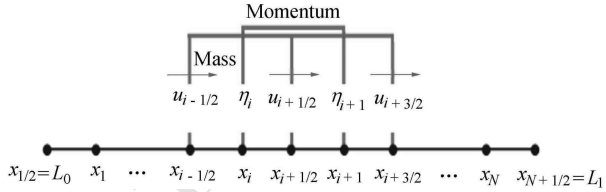

Fig. 5. Discretization of staggered conservative scheme

The scheme leads to the numerical solutions of Eq. (1):

$$\eta_i^{n+1} = \eta_i^n - \frac{\Delta t}{\Delta x}\left(h_{i+1/2}^{*n} u_{i+1/2}^n - h_{i-1/2}^{*n} u_{i-1/2}^n\right) \tag{28}$$

$$u_{i+1/2}^{n+1} = u_{i+1/2}^n + g\frac{\Delta t}{\Delta x}\left(\eta_{i+1}^{n+1} - \eta_i^{n+1}\right) \tag{29}$$

where superscripts and subscripts denote the time step and spatial grid point, respectively. As seen from Eq. (28), the water depth, h^*, is required at half-grid points and is unknown. The value of h^* is approximated using a first-order upwind scheme and is chosen depending on the flow velocity as follows:

$$h_{i+1/2}^* = \begin{cases} h_i & u_{i+1/2}^n \geq 0 \\ h_{i+1} & u_{i+1/2}^n < 0 \end{cases} \tag{30}$$

For positive flow, Eq. (28) becomes

$$\eta_i^{n+1} = \eta_i^n - \frac{\Delta t}{\Delta x}\left(h_i^n u_{i+1/2}^n - h_{i-1}^n u_{i-1/2}^n\right) \tag{31}$$

Note that on the right-hand side of the momentum equation (Eq. (1)), η is calculated at t_{n+1}, instead of at t_n, as this choice is required to maintain the stability of the scheme. Using Von Neumann stability analysis, the system is stable if $|\lambda| < 1$, where λ is the eigenvalue. The detailed derivation of the stability criteria for the numerical scheme can be found in Appendix A. Both the wave elevation and velocity are set to zero initially. As time passes, the wave is incident from

the left, propagates over the sloping topography, and radiates through the right boundary. The initial and boundary conditions, respectively, are as follows:

$$\eta(x,0)=0 \qquad u(x,0)=0 \tag{32}$$

$$\eta(L_0,t)=A\sin(\omega t) \qquad u(L_1,t)=\eta(L_1,t+\Delta t)\sqrt{\frac{g}{h_3}} \tag{33}$$

where A is the wave amplitude.

4. Results and discussion

To validate the numerical scheme, the numerical results were compared with the analytical solutions and the solution of Bautista et al. (2011). To study the influence of the sloping topography on the transmission and reflection of waves, the following parameter values were chosen. The constant depth h_2 was set as $h_2 = 10$ m, the gravitational acceleration as g = 9.81 m·s^{-2}, the length of the sloping bottom as L = 10 m, the time step as Δt = 0.001 s, and the spatial step length as Δx = 0.025 m. For the calculation, we used a monochromatic wave with a single crest. To calculate the amplitude of the reflected wave, the wave elevation at a certain point before the sloping bottom was observed, and then the maximum amplitude of the wave moving leftward, which was the reflected wave, was recorded. Comparisons of the transmission and reflection coefficients of those solutions are given in Figs. 6 and 7, respectively. Fig. 6 shows that the analytical and numerical solutions of C_T are in agreement. The solutions of C_T obtained in this study converge to that of Bautista et al. (2011) as $\varepsilon \to 1$, where $\varepsilon = h_3/h_2$. It can also be seen in Fig. 7 that the solutions of C_R obtained in this study show the same trend, converging to that of Bautista et al. (2011) as $\varepsilon \to 1$. This is as expected as the WKB solution being valid for $\varepsilon \to 1$. The analytical and numerical solutions obtained in this study are in agreement with each other and extend the solution of Bautista et al. (2011) to the regime in which ε is not close to 1.

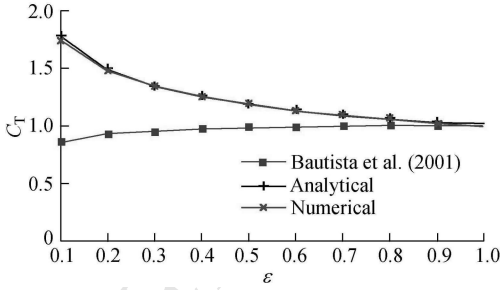

Fig. 6. C_T vs. ε

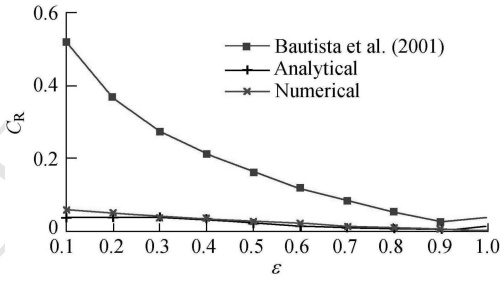

Fig. 7. C_R vs. ε

The differences between solutions, obtained by the analytical and numerical methods, for different values of ε are compared in Table 1, where E_T and E_R are the absolute errors of the numerical results of the transmission and reflection coefficients, compared with their analytical results, respectively, with $E_T = |C_{Tn} - C_{Ta}|$ and $E_R = |C_{Rn} - C_{Ra}|$. C_{Tn} and C_{Ta} are the transmission coefficients obtained by the numerical and analytical methods, respectively; and C_{Rn} and C_{Ra} are the reflection coefficients obtained by the numerical and analytical methods, respectively.

Table 1

Differences between analytical and numerical solutions of transmission and reflection coefficients

ε	E_T	E_R	ε	E_T	E_R
0.100	0.02743	0.01772	0.600	0.00008	0.00614
0.200	0.01001	0.01019	0.700	0.00096	0.00668
0.300	0.00513	0.00116	0.800	0.00103	0.00587
0.400	0.00165	0.00138	0.900	0.00071	0.00430

0.500	0.00254	0.00395	0.999	0.00015	0.00017

It can be clearly seen from the table that the errors are very small. To investigate the accuracy of the numerical scheme proposed in this study, repeated simulations were conducted, with a fixed value of Δx = 0.025 m and Δt ranging from 0.000131 to 0.001831 s, to calculate the error $E_{\mathrm{T}j}$ corresponding to Δt_j and the rate of convergence $\tau_{tj} = \lg\left(E_{\mathrm{T}(j+1)}/E_{\mathrm{T}j}\right)\Big/\lg\left(\Delta t_{j+1}/\Delta t_j\right)$. The results are shown in Table 2. The value of $\left|\tau_{tj}\right|$ is in the range of 0 to 1, indicating that the order of accuracy in the time domain is one.

Table 2

Errors of numerical scheme and convergence rates for different time steps

j	Δt_j (s)	$E_{\mathrm{T}j}$	$\left\|\tau_{tj}\right\|$	j	Δt_j (s)	$E_{\mathrm{T}j}$	$\left\|\tau_{tj}\right\|$
1	0.00013	0.00118	0.0589	5	0.00031	0.00120	0.3171
2	0.00015	0.00119	0.0459	6	0.00046	0.00136	0.9175
3	0.00018	0.00120	0.0000	7	0.00092	0.00072	0.5896
4	0.00023	0.00120	0.0000	8	0.00183	0.00048	

Next, to examine the accuracy of the numerical scheme in the spatial domain, repeated simulations were conducted, with $\Delta t = 0.001$ s and Δx varying between 0.010 m and 1.000 m, to calculate $E_{\mathrm{T}j}$ corresponding to Δx_j and the rate of convergence $\tau_{xj} = \lg\left(E_{\mathrm{T}(j+1)}/E_{\mathrm{T}j}\right)\Big/\lg\left(\Delta x_{j+1}/\Delta x_j\right)$. The results are shown in Table 3. The calculated value of $\left|\tau_{xj}\right|$ is in the range of 1.8 to 2.4, indicating that the order of accuracy in the spatial domain is two. We therefore concluded that the numerical scheme has an accuracy of $O\left(\Delta t, \Delta x^2\right)$ (Pudjaprasetya and Magdalena, 2014; Magdalena et al., 2015).

Table 3

Errors of numerical scheme and convergence rates for different spatial steps

j	Δx_j (m)	$E_{\mathrm{T}j}$	$\left\|\tau_{xj}\right\|$	j	Δx_j (m)	$E_{\mathrm{T}j}$	$\left\|\tau_{xj}\right\|$
1	0.010	0.00000	-	4	0.500	0.01150	2.1479
2	0.025	0.00020	2.3414	5	1.000	0.05097	
3	0.250	0.04390	1.9326				

For a further test, results for a parabolic transition shelf were compared with those of Kajiura (1961). The x-ordinate ran from −100 m to 0 m with x_1 = −60 m and x_2 = −40 m. The parameter a = 0.00625 m^{-1}. The undisturbed water depths in deep and shallow areas were described by $h_2 = ax_1^2$ and $h_3 = ax_2^2$, respectively. The wave propagated from the left with an amplitude of a_{i} = 0.5 m and a wave frequency of ω = 5.9610 s^{-1}. On the right side of the domain, an absorbing boundary condition was applied. The numerical result of the wave transmission coefficient was compared with those obtained by the analytical formula of Eq. (27) and from the literature, as shown in Tables 4 and 5, where C_{Tl} is the wave transmission coefficient calculated from the formula derived by Kajiura (1961) and reproduced by Mei et al. (2005) using asymptotic expansions. The formula is valid only for $x_2 - x_1$ h_2 or h_3, or when the water depth in the transition region with a sloping bottom strictly decreases in the shoreward direction. For example, in the case for x_2 = −50 m in Table 4, where $x_2 - x_1$ = 10 m is less than h_2 = 22.5 m and h_3 = 15.625 m, the value of C_{Tl} is far from the analytical and numerical results, demonstrating that Kajiura's formula is invalid. However, when all the parameters were chosen for the transition region with decreasing water depth under that condition, we could calculate the shoaling coefficient by inversion of the wave transmission coefficient given by Kajiura (1961) (Fig. 4).

Table 4

Comparison of wave transmission coefficients for x_1 = −60 m, a = 0.00625 m^{-1}, and incident wave when a_{i} = 0.5 m and ω = 5.9610 s^{-1}

x_2 (m)	μ	C_{Tn}	C_{Ta}	C_{Tl}
−20	3.0	1.7668	1.7318	1.1764
−30	2.0	1.4049	1.4140	1.0329
−40	1.5	1.2294	1.2247	0.8410
−50	1.2	1.0974	1.0952	2.5570

Table 5

Comparison of wave transmission coefficients for μ = 1.5 and a = 0.00625 m^{-1}

ω (s^{-1})	$\omega^2/(ga)$	C_{Tn}	C_{Ta}	C_{Tl}
4.7688	371.2890	1.2322	1.2247	0.8655
3.5766	208.8500	1.2232	1.2247	0.8436
2.3844	92.8223	1.2359	1.2247	0.8286
1.1922	23.2056	1.2252	1.2247	0.8198

For a final test of the numerical scheme, a case in which the seabed transition was neither linear nor parabolic was chosen. The topography was determined as follows:

$$h(x)=\begin{cases} h_2 & x<80\ \text{m} \\ \dfrac{h_3-h_2}{2}\cos\dfrac{\pi(x-80)}{160-80}+\dfrac{h_3+h_2}{2} & 80\ \text{m}\le x\le 160\ \text{m} \\ h_3 & x>160\ \text{m} \end{cases} \quad (34)$$

Monochromatic waves entered from the left with a wave amplitude of 0.5 m, and water depths were set as h_2 = 22.5 m and h_3 = 10 m. As time passed, the waves propagated to the shallow area and flowed through the right boundary. The computation was carried out in the spatial domain ranging from 0 to 250 m, with a spatial grid size of Δx = 0.01 m. Fig. 8 shows a comparison of the free surface elevation of the numerical solution in this study and the WKB solution described in Kristina et al. (2013). It is hard to distinguish between the two solutions for the free surface elevation in Fig. 8. The WKB and numerical solutions are in close agreement.

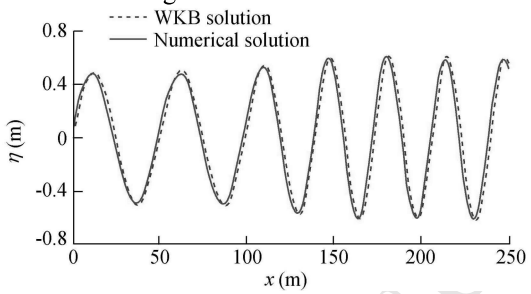

Fig. 8. Free surface elevation of shoaling wave at t = 50 s when h_2 = 22.5 m and h_3 = 10 m

The wave transmission coefficient was calculated for different values of ε. Comparison of the calculated results with those of the WKB solution in Kristina et al. (2013) is shown in Fig. 9.

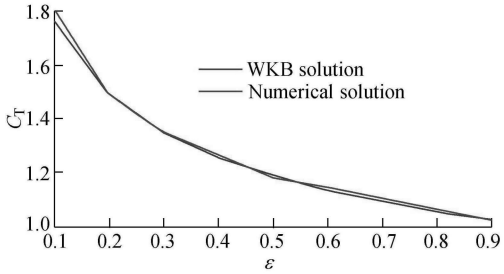

Fig. 9. Wave transmission coefficients determined by numerical scheme and WKB method for ε in [0.1, 0.9]

Finally, the numerical scheme was applied to simulation of the wave shoaling phenomena over a more complex bathymetry: a cross-sectional bathymetry of the coast of Aceh, in Sumatra, Indonesia, where the 2014 Boxing Day tsunami occurred. The cross-section was taken from (95.0278°E, 3.2335°N) to (96.6583°E, 3.6959°N) with Δx = 0.4333 m. The wave propagating over the bathymetry along this cross-section is depicted in Fig. 10. The incident wave with a 1-m wave height and a wave period of 17 min propagated to the shallow-water area. As the water depth decreased, wave shoaling phenomena occurred, with the wavelength shortening and the amplitude increasing. For the domain shown, the water depth was 1047 m in the deep-water region and approximately 30 m in the shallow-water region. The wave height was 2.44 m in the shallow-water region, corresponding to a numerical solution of the wave transmission coefficient of 2.44. The analytical solution gave a transmission coefficient of 2.43 in this study, showing a reasonable agreement with the numerical solution.

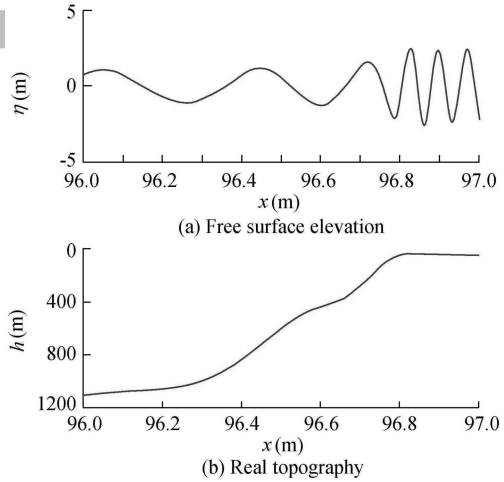

Fig. 10. Transient wave propagating over cross-sectional bathymetry of coast of Aceh

5. Conclusions

In this paper, new analytical solutions for transient long waves shoaling over coastal shelves have been presented. Specifically, expressions for the surface elevation, horizontal velocity, and wave reflection and transmission coefficients have been derived for linear and parabolic transition shelves. Novel results from a numerical scheme have also been presented based on a staggered conservative formulation with upwind updating. The analytical and numerical solutions for several cases show agreement. The solutions obtained in this study have also been compared with previous results from WKB approximations, showing that this study provides a means of extending solutions beyond the normal WKB limits. The numerical scheme was applied to the case of tsunami propagation towards the coast of Aceh, Indonesia. Results obtained from the numerical scheme suggest that waves with a period of 17 min, close to values quoted by Stosius et. al. (2010) for the Boxing Day tsunami, would experience amplification by a factor of 2.44 when traveling into the coastal waters where the depth was 30 m. This coincides with the scale of amplification proposed by Kowalik (2012), suggesting that the relatively simple approach proposed in this paper can provide solutions that are useful in practice, in either an operational or strategic context.

Appendix A: Stability analysis

Here, we derive the stability criterion for Eqs. (28) and (29). Setting $\eta_i^n = \rho^n \mathrm{e}^{\mathrm{i}a'i}$ and $u_{i+1/2}^n = r^n \mathrm{e}^{\mathrm{i}a'(i+1/2)}$ and substituting η_i^n and $u_{i+1/2}^n$ into Eqs. (28) and (29) give the following:

$$\begin{bmatrix} 1 & 0 \\ g\dfrac{\Delta t}{\Delta x}2\mathrm{i}\sin\left(\dfrac{a'}{2}\right) & 1 \end{bmatrix}\begin{bmatrix} \rho^{n+1} \\ r^{n+1} \end{bmatrix} = \begin{bmatrix} 1 & -h_{\max}\dfrac{\Delta t}{\Delta x}2\mathrm{i}\sin\left(\dfrac{a'}{2}\right) \\ 0 & 1 \end{bmatrix}\begin{bmatrix} \rho^{n} \\ r^{n} \end{bmatrix} \tag{A.1}$$

where $\rho = \mathrm{e}^{\mathrm{i}\omega_\mathrm{n}\Delta t}$, with ω_n being the angular frequency of η; $a' = k\Delta x$, with k being the wave number; $r = \mathrm{e}^{\mathrm{i}\omega_\mathrm{r}\Delta t}$, with ω_r being the angular frequency of u; and $h_{\max}$ is the maximum water depth. Eq. (A.1) can be rewritten as

$$\begin{bmatrix} \rho^{n+1} \\ r^{n+1} \end{bmatrix} = \boldsymbol{B}\begin{bmatrix} \rho^{n} \\ r^{n} \end{bmatrix} \tag{A.2}$$

where $\boldsymbol{B}$ is

$$\boldsymbol{B} = \begin{bmatrix} 1 & -h_{\max}\dfrac{\Delta t}{\Delta x}2\mathrm{i}\sin\left(\dfrac{a'}{2}\right) \\ -g\dfrac{\Delta t}{\Delta x}2\mathrm{i}\sin\left(\dfrac{a'}{2}\right) & 1-gh_{\max}\left(\dfrac{\Delta t}{\Delta x}\right)^2 2\sin^2\left(\dfrac{a'}{2}\right) \end{bmatrix} \tag{A.3}$$

The eigenvalue λ of matrix $\boldsymbol{B}$ satisfies the following equation:

$$(\lambda-1)\left(\lambda-1+C^2\right)+C^2=0 \tag{A.4}$$

where $C^2 = h_{\max}g\left(\Delta t/\Delta x\right)^2 4\sin^2\left(a'/2\right)$. If $|C|\le 2$ and $|\lambda|=1$, the stability criterion for Eqs. (28) and (29) is $\left(\Delta t/\Delta x\right)\sqrt{h_{\max}g}\le 1$. In this case, the eigenvalue has a norm value equal to one, so the scheme is non-dissipative.

References

Bautista, E.G., Arcos, E., Bautista, O.E., 2011. Propagation of ocean waves over a shelf with linear transition. Mechanica Computacional, (4), 225-242.

Beji, S., Nadoaka, K., 1997. A time-dependent nonlinear mild slope equation for water waves. Proceedings of the Royal Society of London. Series A: Mathematical, Physical and Engineering Sciences, 453(1957), 319-332. https://doi.org/10.1098/rspa.1997.0018.

Bender, C.M., Orszag, S.A., 1978. Advanced Mathematical Methods for Scientists and Engineers. McGraw-Hill, New York.

Berkhoff, J.C.W., 1972. Computation of combined refraction: Diffraction. In: Proceeding of 13th International Conference on Coastal Engineering, ASCE, pp. 55-69, https://doi.org/10.1061/9780872620490.027.

Carrier, G.F., 1966. Gravity waves of water of variable depth. J. Fluid Mech., 24(4), 641-659. https://doi.org/10.1017/S0022112066000892.

Copeland, G.J.M., 1985. A practical alternative to the mild-slope equation. Coastal Engineering, 9(2), 125-149. https://doi.org/10.1016/0378-3839(85)90002-X.

Dalrymple, R.A., Suh, K.D., Kirby, J.T., Chae, J.W., 1989. Models for very wide-angle water waves and wave diffraction, Part 2: Irregular bathymetry. J. Fluid Mech., 201, 299-322. https://doi.org/10.1017/S0022112089000959.

Ebersole, B.A., 1985. Refraction-diffraction model for linear water wave. Journal of Waterway, Port, Coastal, and Ocean Engineering, 111(6), 939-953. https://doi.org/10.1061/(ASCE)0733-950X(1985)111:6(939).

Kajiura, K., 1961. On the partial reflection of water waves passing over a bottom of variable depth. In: Proceedings of the Tsunami Meetings 10th Pacific Science Congress, IUGG, pp. 206-234.

Kim, H.-S., Jung, B.-S., Lee, Y.-W., 2009. A linear wave equation over mild-sloped bed from double integration. Journal of the Korean Society for Marine Environment & Enrgy, 12(3), 165-172.

Kirby, J.T., 1986. On the gradual reflection of weakly nonlinear Stokes waves in regions of varying topography. J. Fluid Mech., 162, 187-209. https://doi.org/10.1017/S0022112086002008.

Kowalik, Z., 1993. Solution of the linear shallow water equations by the fourth-order leapfrog scheme. JGR: Oceans, 98(C6), 10205-10209. https://doi.org/10.1029/93JC00652.

Kowalik, Z., 2012. Introduction to Numerical Modeling of Tsunami Waves. University of Alaska, Fairbanks.

Kristina, W., van Groesen, B., Bokhove, O., 2013. Modelling of tsunami wave run-up over sloping bathymetry using effective boundary conditions. In: EGU Genereal Assembly Conference Abstracts, Vol. 15, p.453.

Li, B., Anastasiou, K., 1992. Efficient elliptic solvers for the mild-slope equation using the multigrid technique. Coastal Engineering, 16(3), 245-266. https://doi.org/10.1016/0378-3839(92)90044-U.

Li, B., Reeve, D.E., Fleming, C.A., 1993. Numerical solution of the elliptic mild-slope equation for irregular wave propagation. Coastal Engineering, 20(1-2), 85-100. https://doi.org/10.1016/0378-3839(93)90056-E.

Lin, P.Z., Liu, P.L.-F., 1998. A numerical study of breaking waves in the surf zone. J. Fluid Mech., 359, 239-264. https://doi.org/10.1017/S002211209700846X.

Madsen, P.A., Bingham, H.B., Liu, H., 2002. A new Boussinesq method for fully nonlinear waves from shallow to deep water, J. Fluid Mech., 462, 1-30. https://doi.org/10.1017/S0022112002008467.

Magdalena, I., Erwina, N., Pudjaprasetya, S.R., 2015. Staggered momentum conservative scheme for radial dam break simulation. J. Sci. Comp., 65(3), 867-874. https://doi.org/10.1007/s10915-015-9987-5.

Mei, C.C., Stiassne, M., Yue, D.K.-P., 2005. Theory and applications of ocean surface waves. In: Advanced Series on Ocean Engineering: Vol. 23, World Scientific. https://doi.org/10.1142/5566.

Nielson, P. 1983. Analytical determination of nearshore wave height variation due to refraction, shoaling and friction. Coastal Engineering, 7(3), 233-251. https://doi.org/10.1016/0378-3839(83)90019-4.

Nielson, P., 1984. Explicit solutions to practical wave problems. In: Proceedings of the International Conference of 19th Coastal Engineering Conference, Houston, pp. 968-982.

Noviantri, V., Pudjaprasetya, S.R., 2010. The relevance of wavy beds as shoreline protection. In: Proceedings of 13th Asian Congress of Fluid Mechanics, pp.489-492.

Nwogu, O., 1993. Alternative form of Boussinesq equations for nearshore wave propagation. Journal of Waterway, Port, Coastal, and Ocean Engineering, 119(6), 618-638. https://doi.org/10.1061/(ASCE)0733-950X(1993)119:6(618).

Panchang, V., Cushman-Roisin, B., Pearce, B., 1988. Combined refraction-diffraction of short-waves in large coastal regions. Coastal Engineering, 12(2), 133-156. https://doi.org/10.1016/0378-3839(88)90002-6.

Pudjaprasetya, S.R., Magdalena, I., 2014. Momentum conservative schemes for shallow water flows. East Asian Journal on Applied Mathematics, 4(2), 152-165. https://doi.org/10.4208/eajam.290913.170314a.

Radder, A.C., 1979. On the parabolic equation method for water-wave propagation, J. Fluid Mech., 95(1), 159-176. https://doi.org/10.1017/S0022112079001397.

Reeve, D.E., 1992. Bathymetric generation of an angular wave spectrum. Wave Motion, 16(3), 217-228. https://doi.org/10.1016/0165-2125(92)90030-6.

Sadeghian, H., Peyman, B., 2012. Analytical solution of wave shoaling based on cnoidal wave theory. In: Proceedings of 9th International Conference on Coasts, Ports and Marine Structures, Tehran.

Smith, R., Sprinks, T., 1975. Scattering of surface waves by a conical island. J. Fluid Mech., 72(2), 373-384. https://doi.org/10.1017/S0022112075003424.

Stosius, R., Beyerle, G., Helm, A., Hoechner, A., Wickert, J., 2010. Simulation of space-borne tsunami detection using GNSS: Reflectometry applied to tsunamis in the Indian Ocean. Natural Hazards and Earth System Sciences, 10, 1359-1372. https://doi.org/10.5194/nhess-10-1359-2010.

Suh, K.D., Dalrymple, R.A., Kirby, J.T., 1990, An angular spectrum model for propagation of Stokes waves, J. Fluid Mech., 221, 205-232. https://doi.org/10.1017/S0022112090003548.

Synolakis, C.E., 1987. The runup of solitary waves. J. Fluid Mech., 185, 523-545. https://doi.org/10.1017/S002211208700329X.